UNIVERSITY OF LEEDS

This is a repository copy of *Experimental study on operating characteristics of a dual compensation chamber loop heat pipe in periodic acceleration fields*.

White Rose Research Online URL for this paper:
http://eprints.whiterose.ac.uk/169108/

Version: Accepted Version

Article:

Xie, Y, Li, X, Han, L et al. (3 more authors) (2020) Experimental study on operating characteristics of a dual compensation chamber loop heat pipe in periodic acceleration fields. Applied Thermal Engineering, 176. 115419. ISSN 1359-4311

https://doi.org/10.1016/j.applthermaleng.2020.115419

© 2020, Elsevier. This manuscript version is made available under the CC-BY-NC-ND 4.0 license http://creativecommons.org/licenses/by-nc-nd/4.0/.

Reuse

This article is distributed under the terms of the Creative Commons Attribution-NonCommercial-NoDerivs (CC BY-NC-ND) licence. This licence only allows you to download this work and share it with others as long as you credit the authors, but you can't change the article in any way or use it commercially. More information and the full terms of the licence here: https://creativecommons.org/licenses/

Takedown

If you consider content in White Rose Research Online to be in breach of UK law, please notify us by emailing eprints@whiterose.ac.uk including the URL of the record and the reason for the withdrawal request.

White Rose university consortium
Universities of Leeds, Sheffield & York

eprints@whiterose.ac.uk
https://eprints.whiterose.ac.uk/

Experimental study on operating characteristics of a dual compensation chamber loop heat pipe in periodic acceleration fields

Yongqi Xie[a], Xinyu Li[a], Longzhu Han[b,*],

Jianqin Zhu[c], Hui Gao[a], Dongsheng Wen[a,d,]**

[a]School of Aeronautic Science and Engineering, Beihang University, Beijing, 100191, China

[b]School of Biological Science and Medical Engineering, Beihang University, Beijing, 100191, China

[c]National Key Laboratory of Science and Technology on Aero-Engines, School of Energy and Power Engineering, Beihang University, Beijing 100191, China

[d]School of Chemical and Process Engineering, University of Leeds, Leeds LS2 9JT, United Kingdom

[*]Corresponding author: Tel: +86(10) 8233 8952, E-mail: hlz@buaa.edu.cn

[**]Corresponding author: Tel.: +86(10) 8231 7528, E-mail: d.wen@buaa.edu.cn

Abstract: Systematic experiments were firstly designed and conducted to investigate the operating characteristics of a dual compensation chamber loop heat pipe (DCCLHP) under periodic acceleration conditions. A new acceleration test rig was built to generate acceleration magnitude up to 11 g. The heat load ranged from 150 W to 300 W. Three different periodic acceleration patterns, two loading modes and two acceleration directions were used to study their influence on the operating characteristics of the DCCLHP. The results demonstrated that the loop temperature could periodically oscillate with the periodic change of the acceleration. A large acceleration could lead to a high operating temperature. Configuration B could cause the lower operating temperature than configuration A for a fixed case. There were stable operating temperature difference and thermal resistance variation before and after the periodic acceleration acting for the loading mode 1. Temperature overshooting after unloading the periodic acceleration was also confirmed for the loading mode 2. Such phenomena could be explained by the change of the vapor-liquid distribution in the loop and the heat leak from the evaporator to the compensation chambers (CCs). The loop temperature oscillation with different frequency and amplitude might also occur during each periodic acceleration. For the cases of 150 W and configuration A, the acceleration effect could trigger the operating temperature exceeding 60 ^{o}C. Our work proves significant phenomena existing in the DCCLHP and presents detailed analysis, which would be of great importance for the development of new generation of loop heat pipe used in aircraft thermal management system.

Keywords: Loop heat pipe; Dual compensation chambers; Periodic acceleration force; Operating characteristics.

Nomenclature

R	Thermal resistance, K/W
Q_e	Heat load, W
Tin	Inlet temperature of cold plate, K
Tout	Outlet temperature of cold plate, K
$\overline{T}_{cp}$	Average temperature of cold plate, K

Acronyms

CC	Compensation chamber
DCCLHP	Dual compensation chamber loop heat pipe
LHP	Loop heat pipe
RTD	Resistance temperature detector

1. Introduction

With the rapid development of aerospace technology, the conventional cooling technology cannot meet the thermal management demand of electronic devices with higher and higher heat dissipation power. New cooling technique has become an urgent demand for solving the cooling problems [1,2]. Loop heat pipe (LHP), an efficient two-phase heat transfer component, has attracted increasing attentions since it was invented [3,4]. It has many advantages including long heat transport distance, strong anti-gravity ability, high heat transfer efficiency and accurate temperature control ability. With such promising properties, LHP has been widely used in the area of aerospace and terrestrial electronics in recent years [5,6].

LHP is mainly composed of evaporator, condenser, compensation chamber (CC), liquid and vapor transport line. It transports heat by evaporating and condensing the working fluid from the evaporator and condenser, respectively. Nowadays, a large number of experimental and numerical investigations have been conducted on the steady-state operation and startup performance [7-9], structure design [10,11] and internal visualization [12,13] for the LHP with a single cylindrical CC. Previous researches have brought people with deeper insights of the operating principle and heat transfer mechanism.

Compared with the conventional heat pipe, LHP shows its excellence as it overcomes the inherent structural limitations and also retains the merits of the traditional one. High heat transfer ability can be maintained for a long distance in terrestrial gravity due to its special capillary core structure. However, in the thermal tests in gravity, some orientations between evaporator and CCs will occasionally cause the difficulty in supplying the liquid and the LHP even cannot startup. To solve the dilemma, the concept of a dual compensation chamber loop heat pipe (DCCLHP) is proposed. It has two CCs at the both ends of evaporation. Previous studies have investigated the operating characteristics of DCCLHPs. Gluck and Gerhart [14] studied the performance of the DCCLHP using ammonia as working fluid. They found that it could startup and work normally under different configurations between evaporator and CCs. Operation features at nine different orientations were summarized in their study [15]. Long and Ochterbeck [16] experimentally investigated the operating performance of a DCCLHP at transient cyclic heat loads and different orientations, showing that the temperature overshot before starting up increased with the increase of the tilt angle of the evaporator. The performance at constant heat load was similar to that at cyclic heat load with frequency more than 0.1 Hz. The research group led by Lin [17-20] inspected the operating performance systematically and tried to give insight into the operating mechanism of the ammonia-strain-steel DCCLHP. They also confirmed that the DCCLHP could operate normally at any orientation but show different operating performance at different orientations. Based on the visual observations, they observed the flow inside the DCCLHP and investigated the startup behavior, temperature hysteresis and instability. They believed that the different startup performance derived from the change of the vapor-liquid distribution and the heat leak from the evaporator to the CCs. Chang *et al.* [21, 22] experimentally investigated the startup and operating performance of the DCCLHP anti-icing system. Stainless steel with nickel wick was used. Ethanol and ethanol-water mixture were utilized as working fluid. The results showed that the angle attack could significantly affect the operating temperature and led to a temperature oscillation of the anti-icing system. Moreover, the DCCLHP with 60% concentration of mixture operated more robustly and stably than that with pure ethanol.

However, when the aircraft combats or maneuvers, airborne electronic devices suffer from acceleration forces with different directions and magnitudes. Correspondingly, the operating performance of the LHP used to cool the electronic devices will vary. To date there are only a few reports which show the operating performance of the conventional LHP and the DCCLHP subjected to acceleration force. Ku *et al.* [23,24] carried out a series of experiments on a LHP subjected to variable acceleration ranging from 1.2 g to 4.8 g. It was found that the LHP could startup and operate under all working conditions. The temperature oscillation was also observed. Fleming *et al.* [25] studied the operation characteristics of titanium-water based LHP under standard and elevated acceleration fields. In their works, the heat load on evaporator and CC was 100 W-600 W and 0-50 W, respectively. The radial acceleration ranged from 0 to 10 g. The results proved that the dry-out conditions occurred more readily with the heat load between 100 W and 400 W. The radial acceleration had little effect on the thermal resistance and evaporative heat transfer coefficient of the LHP. Yerkes *et al.* [26,27] studied the operating performance of a LHP via experiment under combined steady-periodic acceleration and constant heat load conditions. They found that the periodic acceleration force with greater frequency and peak-to-peak amplitude showed less detrimental impact on the LHP performance. If decreasing frequency and increasing peak-to-peak amplitude, however, detrimental impact on that aggravated. In addition, the transient operating performance of a titanium-water based LHP subjected to a phase-coupled evaporator heat input and acceleration field was studied in detail [28]. It was found that the condenser temperature and phase angle could change the time of LHP operating failure. Xie *et al.* [29,30] carried out experimental studies on the operating behaviors of a stainless steel-ammonia DCCLHP under terrestrial gravity and constant acceleration conditions. The results revealed that the transition of the operation mode was a function of acceleration direction, magnitude and heat load. The DCCLHP could startup and operate normally even the acceleration was up to 11 g. Acceleration effect significantly affects the startup performance at small heat load. Besides, reverse flow, temperature oscillation and evaporation in the evaporator core phenomena were observed.

To the best of our knowledge, there are no detailed experimental data available in literatures concerning the effect of the varied acceleration force on the DCCLHP, especially the periodic acceleration force. Therefore, our study aims to provide comprehensive experimental data exploring the transient operating performance of a DCCLHP under periodic acceleration conditions. Three different periodic acceleration patterns with different acceleration magnitudes, two loading modes with different heat loads and accelerations as well as two acceleration directions are applied, compared and analyzed in this work.

2. Experimental apparatus and test parameters

2.1 Experimental apparatus

The experiment to investigate the operating performance of the DCCLHP under periodic acceleration force was performed at the Reliability and Environmental Engineering Laboratory at BeiHang University, Beijing, China. Fig. 1 presents the schematic diagram of the experimental test rig which mainly includes cooling water circulation subsystem, data acquisition and control subsystem, acceleration simulating and control subsystem as well as test section.

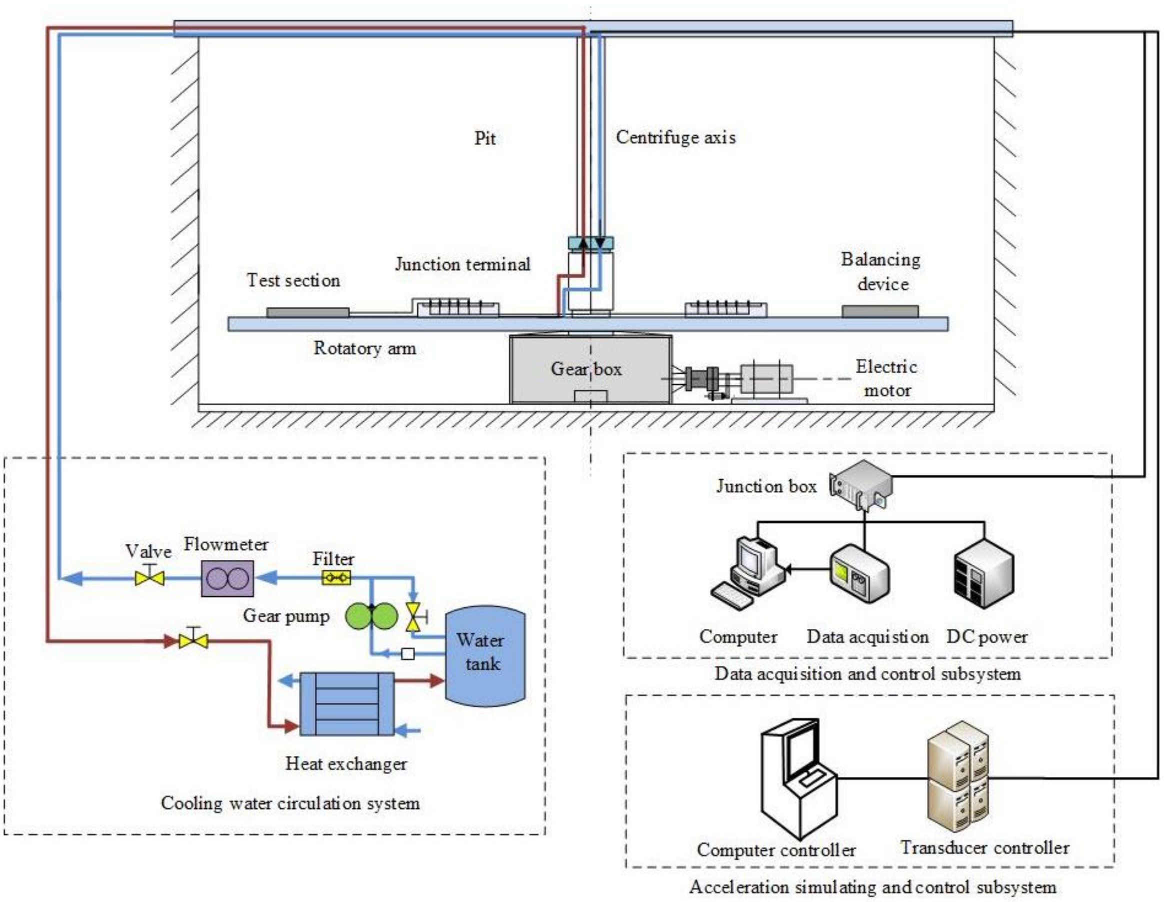

Fig.1 The structure of the experimental system.

In order to avoid the interaction of each component under acceleration field, only test section including the DCCLHP and a cold plate was arranged on the rotational arm. The other devices were placed on a stationary console. The cooling water circulation subsystem mainly consists of a thermostatic water tank, gear pump, mass flow rate (DMF-1-2), plate heat exchanger and cold plate. The gear pump driven by a variable-frequency driver circulated the cooling water in the loop. The thermostatic water tank provided the cooling water with a constant temperature at 19 ^{o}C. The accurate flow rate was measured by mass flow meter based on Coriolis force with an accuracy of ± 0.5%. The heat from the DCCLHP was transferred to the cooling water inside the aluminum cold plate (type 6061). Then the cooling water was cooled to a lower temperature after flowing through the plate heat exchanger. Finally, the cooled water returned back to the thermostatic water tank.

In the data acquisition and control subsystem, the DC power supply (DH1716A-13) provided constant voltage and current to the flexible polyimide film electric resistance heater, which was adhesively attached on the outer surface of the evaporator of the DCCLHP. The heat load ranging from 0 to 400 W could be applied to the evaporator by changing the output voltage and current within the range of 0-250 V and 0-5 A, respectively. Resistance temperature detectors (RTDs) Pt100 were used to measure the temperature of the DCCLHP, inlet and outlet temperature of the cold plate, and ambient temperature. These temperatures and mass flow rate were recorded by the Agilent 34970A and saved in a remote computer placed in the control room.

The acceleration simulating and control subsystem provided the required acceleration force, which was generated by the rotational arm of the centrifuge spinning clockwise. An electric motor drove the rotational arm to rotate by a gear box. These facilities were installed in a pit and controlled by a remote computer controller and transducer controller. The acceleration magnitude and actuation duration were set by the computer controller. To get the required acceleration magnitude up to 11 g, the test section should be arranged on a set location on the rotational arm. The accuracy of the acceleration is ± 5% of the given value. The continuous operation duration of the centrifuge was no more than 1 hour for the issue of safety. The stationary and rotational parts of the water loop tubes, signal wires and electrical wires for heating were linked up by the liquid collecting ring and the electric slip ring, respectively. Both the liquid collecting ring and the electric slip ring installed in the centrifuge axis were specially designed to ensure the flow and electric current working properly as the rotational arm was rotating during the test. Fig. 2 depicts a photo of the centrifuge and the test section horizontally arranged on the rotational arm.

In the test section, a stainless steel-ammonia DCCLHP manufactured in the China Academy of Space Technology was horizontally installed in a stainless steel enclosure. The filling quantity of working fluid was insufficient which means that the evaporator core could not be full of liquid under all conditions. Fig. 3 shows a picture of the test object and the internal construction of the evaporator and the CCs. The overall dimension of the DCCLHP is 565 mm × 469 mm × 25 mm. The major design parameters of the test DCCLHP are summarized in Table 1.

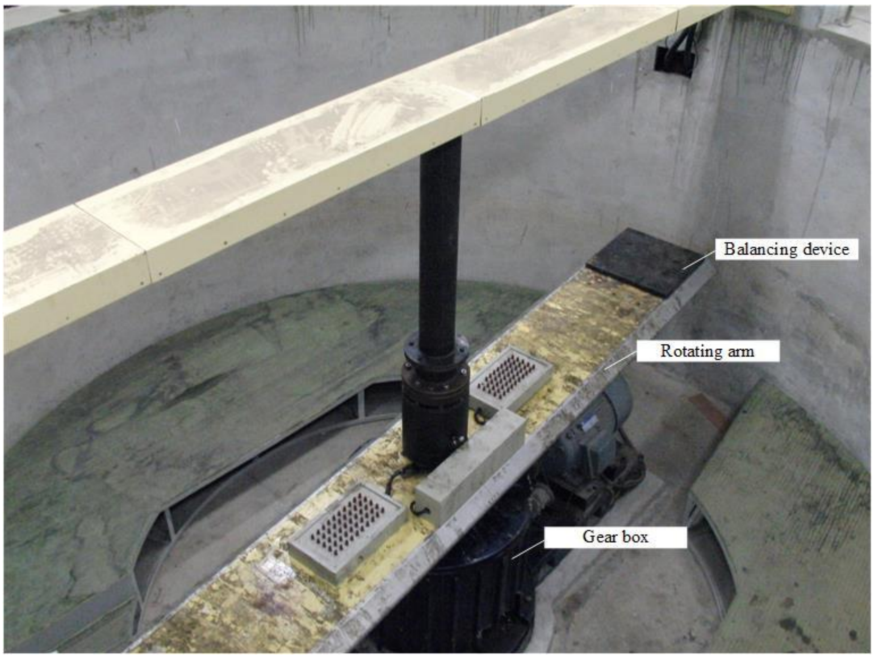

Fig.2 The diagram of the centrifuge.

As shown in Fig. 3 (a), the bayonet passed through one CC and was extended to the middle point of the evaporator core to discharge the vapor bubbles from the evaporator core at any arrangement orientation. A nickel wick with a pore radius of 1.5 μm was used only in the evaporator. The vapor line, liquid line and condenser line were all smooth round stainless steel tubes with an outer diameter of 3.0 mm. The condenser line was welded to six copper fins which were fixed on the top surface of the cold plate with screws, as shown in Fig. 3 (b). Moreover, the thermal conductive grease was used between the copper fins and the cold plate to decrease the contact thermal resistance. In order to reduce the heat transfer between the DCCLHP and the surroundings, the whole DCCLHP were wrapped with insulation materials and the stainless steel enclosure was crammed with glass wool.

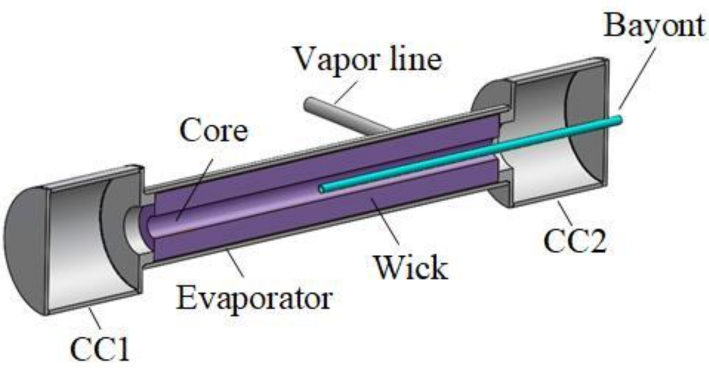

(a) Internal structure of the evaporator

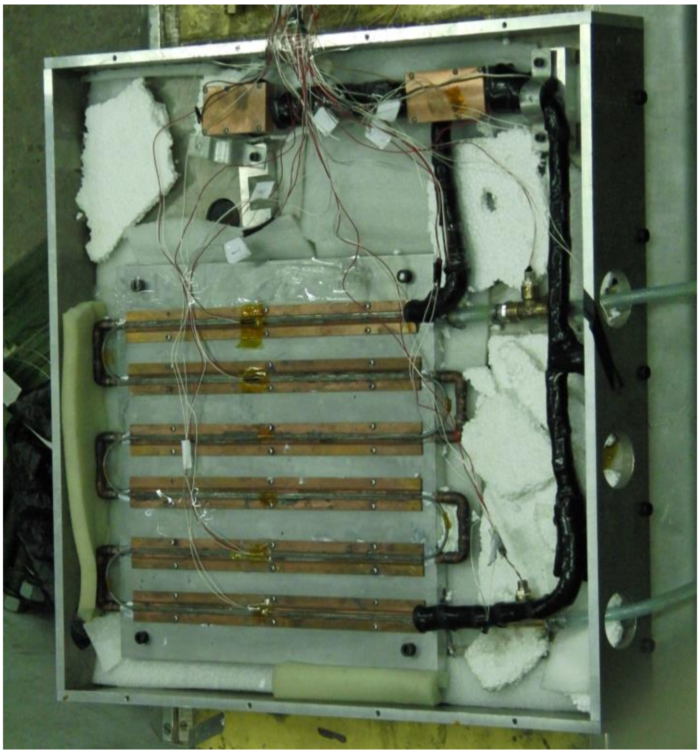

(b) A photo of the test DCCLHP

Fig.3 A photo of the test DCCLHP and internal structure of the evaporator

Table 1 Major design parameters of the test DCCLHP.

Evaporator	O.d/i.d. × length of casing	20 mm/18 mm×209 mm
	Material	Stainless steel
Wick	Pore radius	1.5 μm
	Porosity	55%
	Permeability	>5×10^{-14} m^2
	O.d/i.d. × length	18 mm/6 mm×190mm
	Material	Nickel
Vapor line	O.d/i.d. × length	3 mm/2.6 mm×225 mm
	Material	Stainless steel
Liquid line	O.d/i.d. × length	3 mm/2.6 mm×650 mm
	Material	Stainless steel

Condenser line	O.d/i.d. × length	3 mm/2.6 mm×2200 mm
	Material	Stainless steel
CCs	O.d/i.d. × length	27 mm/25 mm×64 mm
	Material	Stainless steel
Working fluid	Ammonia	

When the test section was fixed on the end of the rotational arm, non-uniform radial acceleration forces on the DCCLHP were generated at different radius positions. GB/T2423.15 requires that the acceleration magnitude should range from 90% to 130% related to the value at a certain rotational radius over the DCCLHP. Thus, the DCCLHP should be installed at approximate 1.9 m of rotational radius of the centrifuge. Correspondingly, the value of the rotational radius should also be set to 1.9 m in the acceleration control software.

In the current study, fourteen RTDs were utilized to monitor the temperature in the test. Fig. 4 shows the RTD locations of the measuring points along the DCCLHP. RTD1 and RTD2, RTD4 and RTD5 were attached to the top and bottom of the outer surface of CC1 and CC2, respectively. RTD3 was located at the middle position on the evaporator. RTD6 was located at the end of the vapor line, and that is at the inlet of the condenser. RTD7 and RTD8 were located on the condenser line, respectively. RTD9, RTD10 and RTD11 were located at the inlet, middle and outlet position of the liquid line, respectively. RTD12 and RTD13 were used to measure the cooling water temperatures at the inlet and outlet of the cold plate, respectively. RTD14 was used to monitor the ambient temperature.

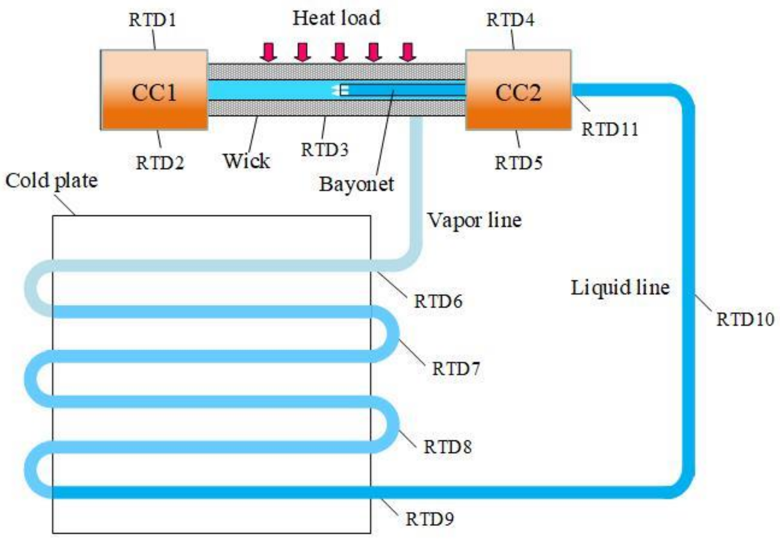

Fig.4 Schematic diagram of RTDs locations on the DCCLHP.

2.2 Test parameters

In the current work, tests were conducted with the following two different configurations, namely configuration A and B as shown in Fig. 5. For both configurations, the DCCLHP was placed on a horizontal plane and the longitudinal axis of the evaporator and CCs was aligned with the direction of the radial acceleration. The main difference for both configurations was that the radial acceleration direction pointed from CC1 to CC2 for configuration A while it pointed from CC2 to CC1 for configuration B.

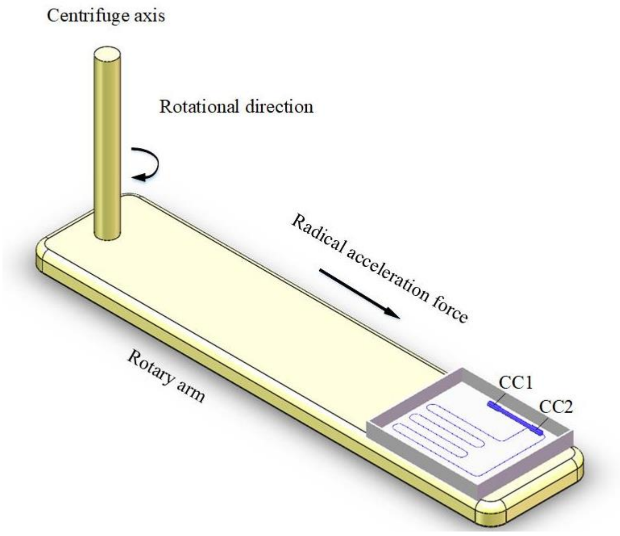

(a) Configuration A

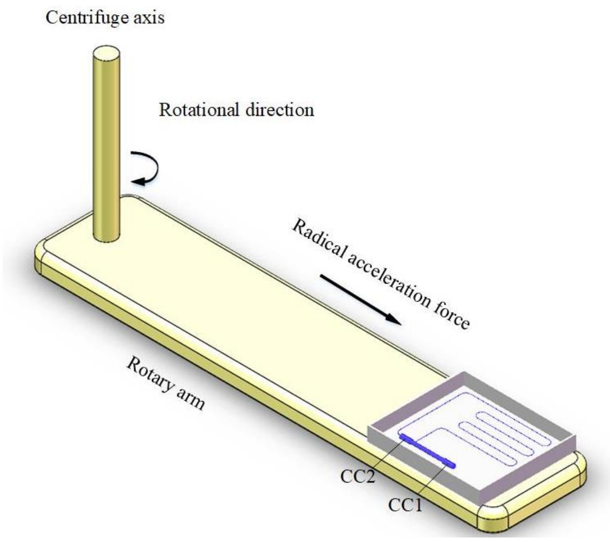

(b) Configuration B.

Fig.5 Two different acceleration directions.

Two loading modes, *i.e.*, loading mode 1 and loading mode 2, were used to apply the heat load and acceleration force on the DCCLHP. For loading mode 1, the heat load was applied on the evaporator firstly and then the acceleration force was applied until the DCCLHP reaching a steady state. For loading mode 2, the heat load and the acceleration force were acted on the DCCLHP simultaneously. The heat load ranged from 150 W to 300 W and the acceleration magnitude from 0 g to 11 g. Moreover, three different periodic acceleration force were generated and used to study the effect on the operating performance of the DCCLHP. Fig. 6 presents these periodic acceleration patterns in the tests. In each periodic acceleration pattern, the action time of the acceleration force was 5 minutes. In periodic acceleration pattern 1, 0 g referred to no acceleration action but only the gravity and the lasting time was 1 minute. In order to compare different cases, the cooling water temperature at the inlet of the cold plate was kept at 20.3 ± 0.5 °C. The indoor temperature was kept at about 26 °C.

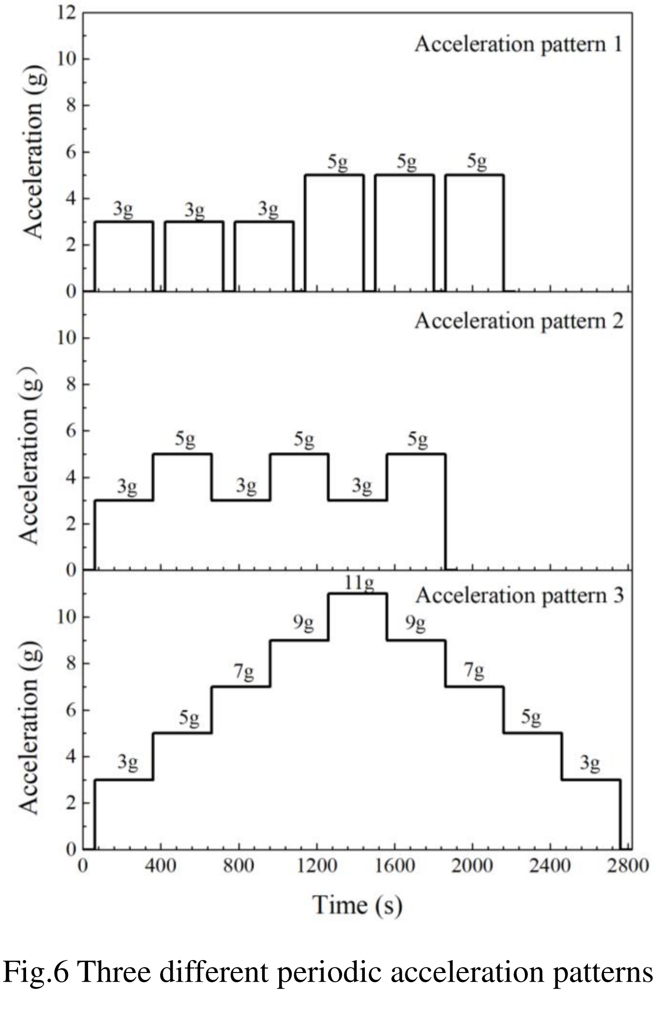

Fig.6 Three different periodic acceleration patterns.

2.3 Test procedure

Calibrations of the RTDs and mass flow meter were conducted prior to the formal test. The validation of the experimental setup was verified by measuring the thermal conductivity of a pure copper bar with the diameter of 30 mm under terrestrial gravity conditions. Detailed descriptions are available in Ref. [30].

Before each test, the test section was arranged at a proper location on the rotational arm for the given acceleration direction. When starting the formal tests, the data acquisition and control subsystem was firstly operated and then the cooling water circulation subsystem was turned on. The cooling water circulated until the system reaching a steady state. Consequently, for the loading mode 1, the DCCLHP first operated to a steady state at a given heat load on the evaporator and then the acceleration simulating and control subsystem started to apply the acceleration force. While for the loading mode 2, the film heater and the centrifuge were turned on simultaneously. Then the effect of different magnitudes and directions of the periodic acceleration force, and that of different heat loads on transient operating performance was investigated.

3. Results and discussion

The operating performances of the DCCLHP subjected to various periodic acceleration patterns and loading modes are presented in the following sections, including several particular phenomena such as stable operating temperature difference, temperature overshooting after unloading, temperature oscillation and excessive operating temperature.

3.1 Operating performance during periodic acceleration

In order to analyze the operating performance of the DCCLHP under different periodic acceleration conditions, Fig. 7 depicts the loop temperature profiles at 150 W and loading mode 1 under configuration B and the periodic acceleration pattern 1, 2 and 3, respectively. Such results revealed that the loop temperature under periodic acceleration conditions was obviously lower than that without periodic acceleration force acting. The loop temperature showed periodic oscillation with the acceleration periodic change. Moreover, the temperature oscillation at the acceleration pattern 1 was more than that at the acceleration pattern 2 and 3. The higher the acceleration magnitude, the higher the operating temperature.

As shown in Fig. 7 (a), the loop temperature showed a periodic fluctuation under the periodic acceleration force conditions. Before applying the first 3 g of the acceleration force, the evaporation temperature indicated by RTD3 was 55.1 ^{o}C. The upper and lower surface temperature of the CC1 and CC2 was 54.2 ºC, 53.3 ºC, 46.8 ºC and 37.1 ºC, respectively. The temperature of RTD1 to RTD4 dropped rapidly while the RTD5 temperature increased instantly and then decreased quickly upon applying the periodic acceleration force. The main reason for this was that the vapor-liquid distribution in the loop was changed by the acceleration force, which directed from the CC2 to CC1 under configuration B. It enabled more liquids with lower temperature to enter the CC1 but more vapor with higher temperature to enter the CC2. Consequently, the CC1 temperature decreased while the RTD5 temperature rose rapidly. Moreover, the significant increase of the RTD7 temperature and the slight increase of both RTD8 and RTD9 indicated that the vapor-liquid interface moved forward to somewhere between RTD7 and RTD8 from that between RTD6 and RTD7. The acceleration effect enlarged the area of two-phase region in the condenser. According to the temperature variation of RTD7, RTD8 and RTD9, it could be further inferred that the vapor-liquid interface located closer to the RTD7 point. Thus, the external loop pressure drop caused by acceleration could be neglected. Because the vapor-liquid distribution in the CCs contributed to decreasing the heat leak from the evaporator to the CCs, and thereby the temperature of the evaporator and the CCs dropped continuously.

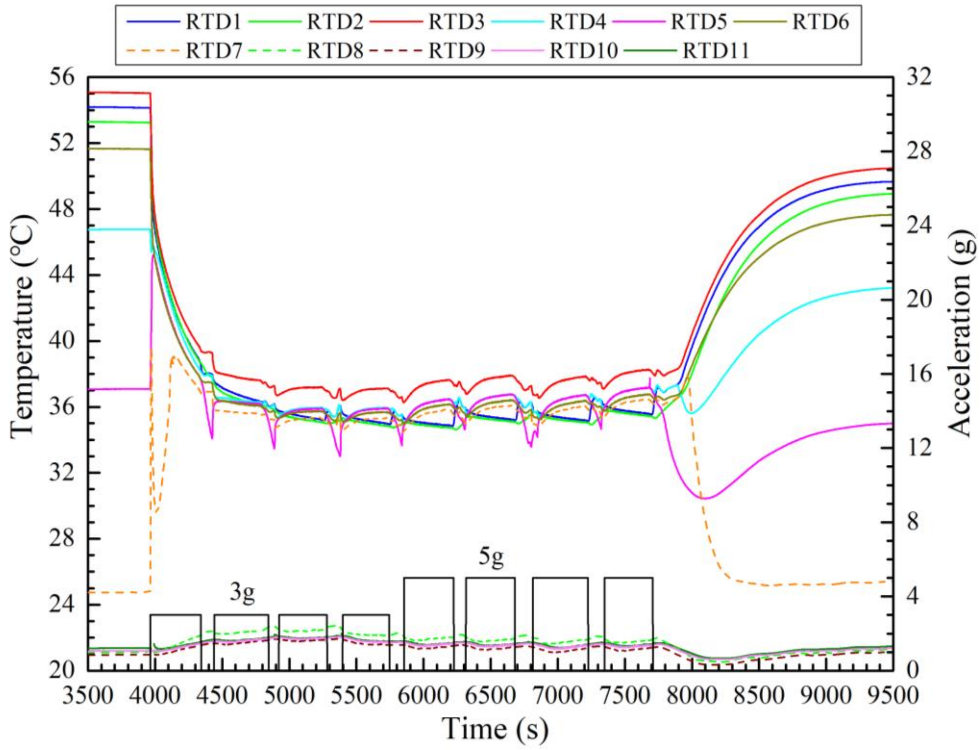

(a) Temperature profiles at acceleration pattern 1

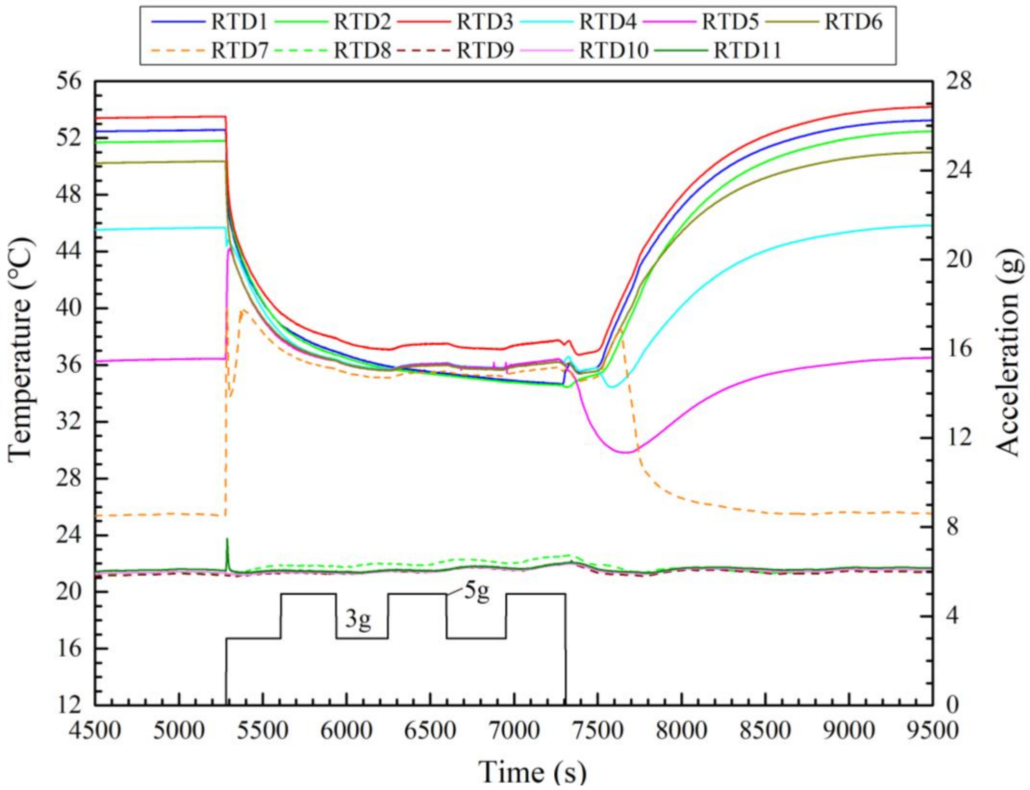

(b) Temperature profiles at acceleration pattern 2

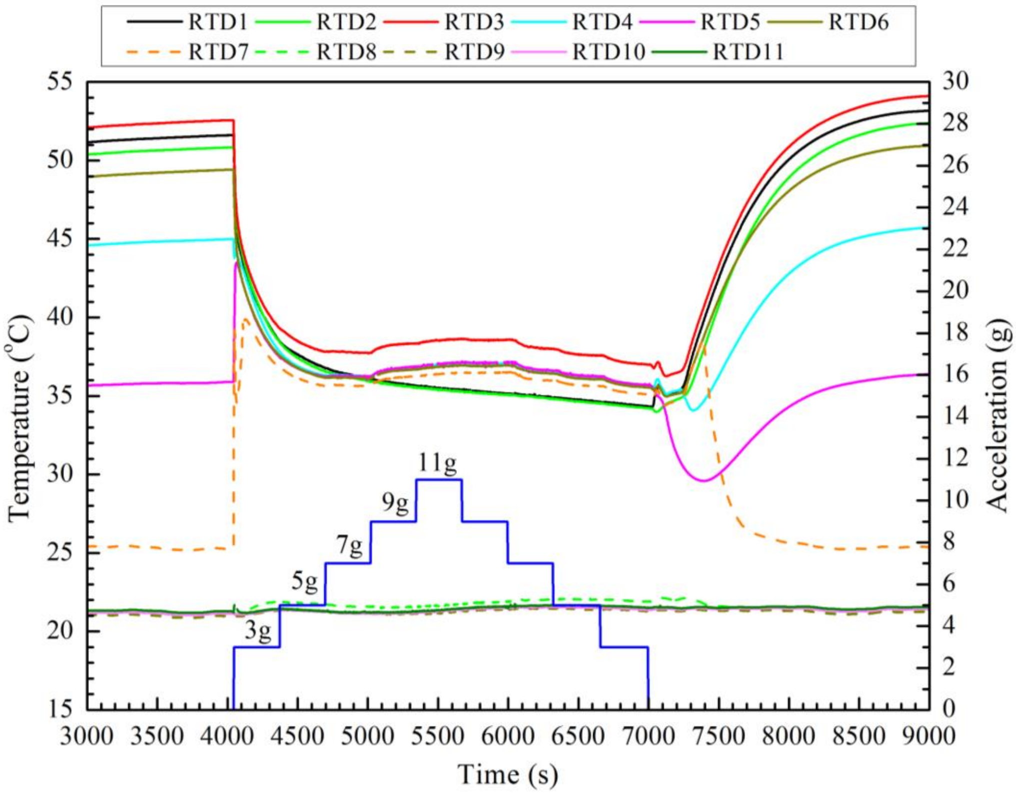

(c) Temperature profiles at acceleration pattern 3

Fig.7 Temperature curves at 150 W, loading mode 1 under configuration B and acceleration pattern 1, 2 and 3.

After unloading the first 3 g，the temperature of RTD1 to RTD4 rose but RTD5 dropped obviously. The reason could be that the vapor-liquid distribution in the loop was quickly altered to the previous state as the acceleration was removed. Hence the heat leak from the evaporator to the CCs increased. Due to the slight change of RTD11 temperature, the subcooling of the returning liquid kept almost constant. Thus, both CCs temperature rose and the evaporator temperature increased accordingly.

When the second 3 g acceleration functioned, the vapor-liquid distribution changed again which would be similar to that in the first 3 g process. The temperature of RTD1 to RTD4 dropped and then kept constant while the RTD5 temperature rose to a constant. Moreover, the loop temperature decreased again as the second 3 g was removed. Similarly, the temperature of the evaporator and the CCs during the period from the third 3 g to the fourth 3 g showed the similar variation as the second 3 g. The evaporator temperature varied from 36.4 °C to 37.2 °C. When 5 g was applied, it could be found that the operating temperature was nearly 0.6 °C higher than that under 3 g at a steady state. The temperature of RTD4 to RTD7 showed similar profiles. This indicated that larger acceleration could result in a higher operating temperature and temperature variation.

After the periodic acceleration was unloaded at about 7674 s, the whole loop operated in terrestrial gravity. The vapor-liquid distribution in the loop recovered back to the initial state before the acceleration was applied. The temperature of the evaporator and the CCs started to increase after a slight fluctuation. Finally, the whole loop reached a steady state. The final operating temperature was 50.5 °C, which was 4.6 °C lower than the initiate temperature.

In Fig. 7 (b), as the first 3 g was applied, the evaporator and the CC1 temperature decreased rapidly, while the upper surface temperature of the CC2 increased firstly and then descended. The RTD7 temperature increased significantly. Meanwhile the RTD8 and RTD9 temperature only changed slightly. It indicated that the vapor-liquid interface was supposed to locate somewhere between RTD7 and RTD8. The acceleration effect altered the vapor-liquid distribution in the loop and further caused the heat leak from the evaporator to the CCs change. Consequently, the loop temperature varied dramatically. During the period of the first 5 g and the second 3 g, the loop temperature dropped continuously except for the RTD8, RTD9 and RTD11 temperature. However, during the period of the second 5 g and the third 3 g and 5 g, the temperature of the evaporator, the CC2 and the liquid line showed a slight increase or decrease as the acceleration increased or decreased. The evaporator temperature changed between 37.0 °C and 37.9 °C. After unloading the acceleration force, the temperature of the evaporator and the CCs increased and finally stayed constant.

In Fig. 7 (c), the loop temperature change presented a similar trend to that shown in Fig. 7 (a) and (b). Especially when the first 3 g and 5 g were applied, all the loop temperature was almost the same with that shown in Fig. 7 (c). When the acceleration magnitude increased to 7 g, the evaporator temperature decreased to about 37.8 °C. However, the evaporator temperature increased continuously up to about 38.6 °C as the acceleration magnitude further increased to 9 g and 11 g. Consequently, the temperature of RTD4 to RTD7 also increased slightly. When the acceleration magnitude decreasing from 11 g to 3 g, the evaporator temperature dropped gradually to about 36.8 °C. During the whole period of the periodic acceleration, the CC2 temperature dropped continuously and the RTD8 to RTD11 temperature kept almost constant. After unloading the acceleration force, the loop temperature presented the similar trend to that shown in Fig. 7 (b). Finally, the temperature of the evaporator and the CCs increased to constant.

In addition, it is worth noting that the operating temperature at 150 W, 200 W and 250 W was lower than that before applying the acceleration force for the cases at the loading mode 1 and configuration B. The operating temperature increased periodically with the periodic acceleration force at almost all cases under configuration A. Some cases showed an excessive operating temperature, which would be discussed in the section 3.5.

Fig. 8 presents the maximum operating temperature of the DCCLHP during the periodic acceleration with the heat load under configurations A and B respectively. Here, the maximum value of the operating temperature was used during the periodic acceleration except for the initiate stage. For the cases at 150 W/loading mode 1, 250 W/acceleration pattern 3/loading mode 1, as well as 150 W/acceleration pattern 3/loading mode 2, the maximum operating temperature of the DCCLHP under configuration A exceeded the maximum allowable temperature of 60 °C. It can be found from Fig. 8 that the maximum operating temperature decreased with the increase of heat load under configuration A for both loading modes. But it firstly decreased and then increased with the heat load under configuration B. For three acceleration patterns, the maximum operating temperature at loading mode 1 was generally greater than that at loading mode 2 under both configurations A and B.

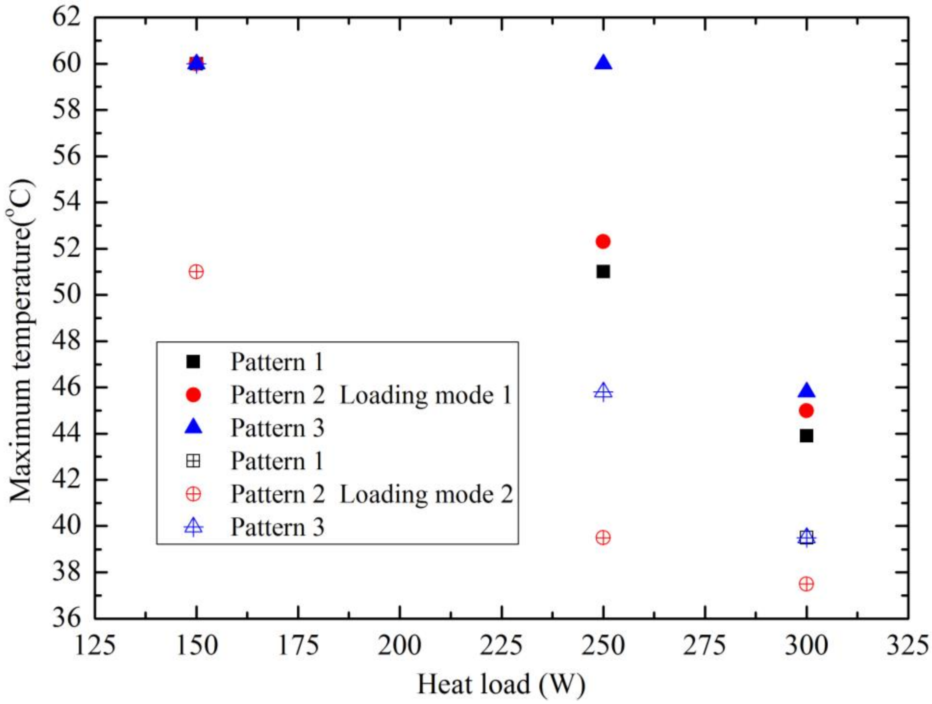

(a) Under configuration A

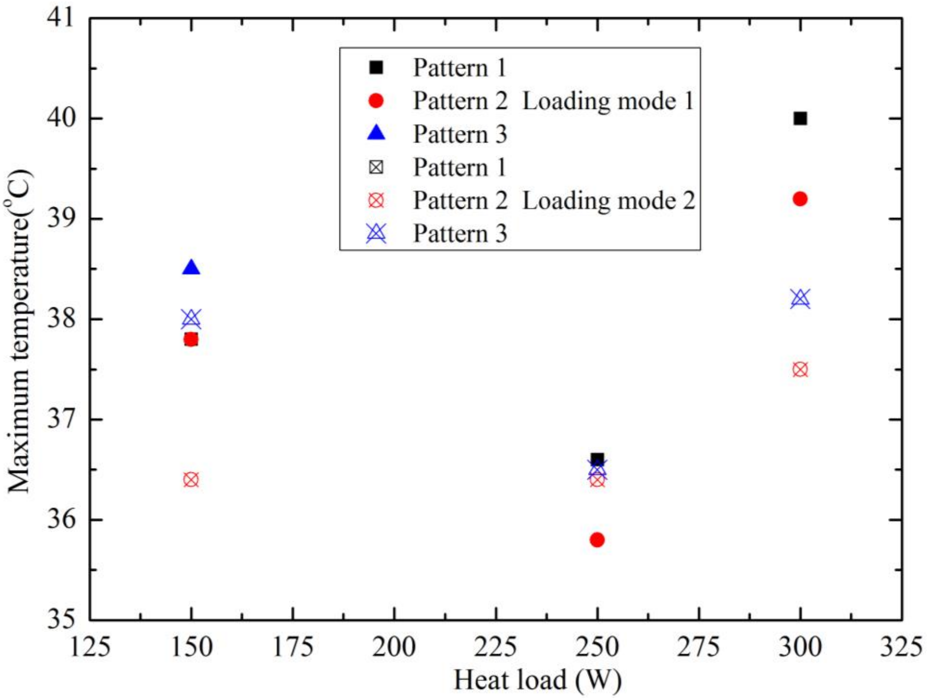

(b) Under configuration B

Fig. 8 Maximum operating temperature during periodic acceleration with heat load under configurations A and B

In Fig. 8 (a), with the heat load of 150 W and loading mode 1, the maximum operating temperature exceeded 60 ºC for three acceleration patterns. For the heat load of 250 W and 300 W, the maximum operating temperature at acceleration pattern 3 was generally higher than that at acceleration pattern 2, which was higher than that at the acceleration pattern 1. For the cases of loading mode 1 at 300 W, the maximum operating temperature at the acceleration pattern 1, 2 and 3 was 43.9 °C, 45 °C and 45.8 °C, respectively. For the cases of loading mode 2 at 300 W, in contrast, it was 39.5 °C, 37.5 °C and 39.5 °C, respectively.

Compared to the cases shown in Fig. 8 (a), the maximum operating temperature under configuration B shown in Fig. 8 (b) was significantly lower than that under configuration A. The maximum temperature at the loading mode 1 and 2 for different heat loads was less than 40 °C and 38.5 °C respectively. For the cases of 250 W and 300 W, the maximum operating temperature at the acceleration pattern 1 was higher than that at the acceleration pattern 2 as the loading mode 1 was used, which showed an opposite trend with those under configuration A. However, for the loading mode 2, the maximum operating temperature at the acceleration pattern 3 was hiher than that at the acceleration pattern 2. It presented the same change to that under configuration A. The maximum operating temperature at the acceleration pattern 1 and 2 under 250 W and loading mode 1 was 36.6 °C and 35.8 °C, respectively. The maximum operating temperature at the acceleration pattern 2 and 3 was 36.4 °C and 36.5 °C for the loading mode 2 at 250 W respectively.

The study on the effect of the loading mode revealed that the maximum operating temperature at 150 W and the loading mode 1 exceeded 60 °C for all the three acceleration patterns. The DCCLHP showed high operating temperature beyond 50 °C for the cases of 250 W and the loading mode 1. For different heat loads, the maximum operating temperature at the loading mode 1 was higher than that at the loading mode 2 in general when the acceleration pattern 1 was applied. For the given heat load, loading mode and acceleration pattern, the maximum operating temperature under configuration A was greater than that underconfiguration B. The maximum temperature under configuration B was less than 40 °C. Moreover, under configuration A, the maximum operating temperature of the acceleration pattern 3 was the highest, followed by the acceleration pattern 2 and the smallest of the acceleration pattern 1. Under configuration B, the maximum operating temperature of the acceleration pattern 1 at the loading mode 1 was more than that of the acceleration pattern 2. For the cases of the loading mode 2, the maximum operating temperature of the acceleration pattern 3 was greater than that of the acceleration pattern 2.

3.2 Stable operating temperature difference

For some cases as the loading mode 1 was used, the steady operating temperature of the DCCLHP before applying acceleration force was different from that after unloading acceleration force, although all the conditions like the heat load, the heat sink temperature and the ambient temperature were identical. As shown in Fig. 7, the steady operating temperature difference before and after the periodic acceleration force was 4.6 ^{o}C, -0.7 ^{o}C and -1.6 ^{o}C for the acceleration pattern 1, 2 and 3, respectively.

Fig. 9 shows the loop temperature profiles at 250 W, periodic acceleration pattern 2 and loading mode 1 under configuration B. It could be clearly seen from Fig. 9 that the operating temperature of the DCCLHP under acceleration conditions was lower than that in gravity. The operating temperature after removing acceleration force was higher than that before applying acceleration force and showed a slight oscillation. The loop temperatures showed periodic oscillation along with the periodic acceleration force. Especially for the temperature of the liquid line, it oscillated more significantly than that shown in Fig. 7 (a).

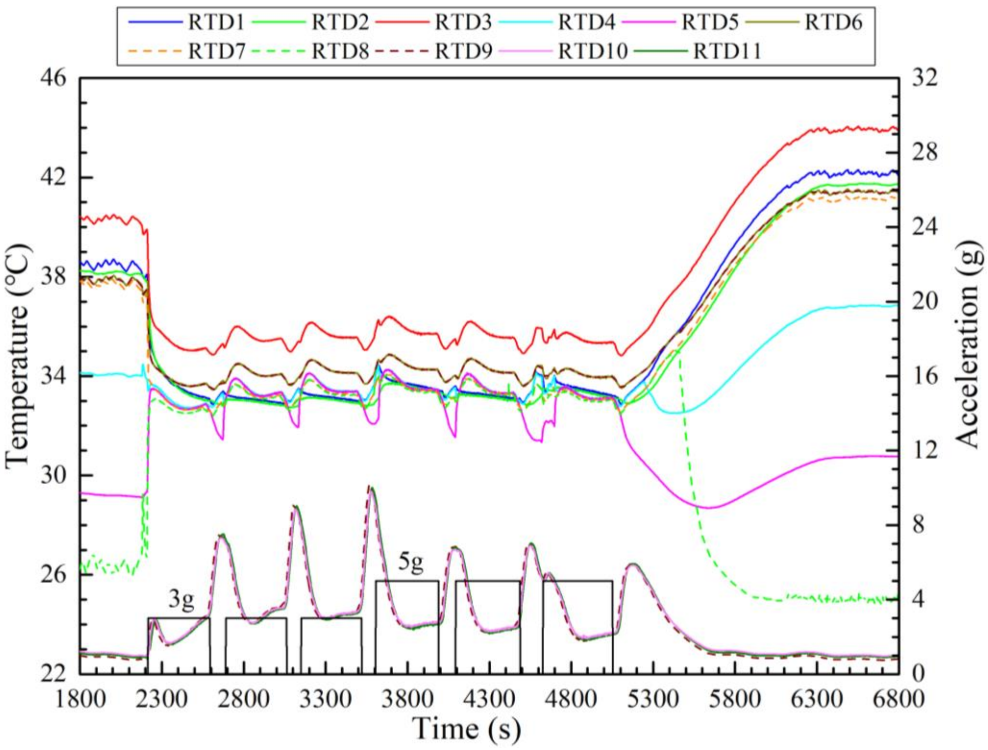

Fig. 9 Temperature profiles at 250 W, acceleration pattern 1 and loading mode 1 under configuration B.

Compared to the case shown in Fig. 7, the temperature changes of the evaporator and the CCs were similar after applying the periodic acceleration. But the temperature amplitude of the evaporator and CCs was larger for the case given in Fig. 9. Furthermore, the vapor-liquid interface moved forward to somewhere between RTD8 and RTD9. A large temperature oscillation of RTD9 to RTD11 indicated that the subcooling of the returning liquid varied acutely. During almost all the periods between two periodic accelerations, the temperature of RTD9, RTD10 and RTD11 increased rapidly. As a result, the evaporator temperature increased and the vapor-liquid interface moved forward. But the subcooling of the returning liquid decreased. On the contrary, if the periodic acceleration (3 g or 5 g) existed, the vapor-liquid interface would move backwards, which induced an increase of the subcooling of the returning liquid. Additionally, the peak value of the RTD11 temperature corresponded to the valley value of the upper surface of the CC2. And at these moments, the acceleration was just applied. It was at about 6400 s that the whole loop reached a quasi-stable state again. The operating temperature was about 43.9 °C. It showed an increase of 3.5 °C relative to 40.4 °C before the periodic acceleration.

Fig. 10 shows the operating temperature and thermal resistance of the DCCLHP before and after the periodic acceleration patterns under both configurations and loading mode 1 conditions. Here, the thermal resistance of the DCCLHP was determined by the evaporator temperature and the average temperature of the cold plate.

$$R = \frac{T_{\mathrm{e}}\text{-}\overline{T}_{\mathrm{cp}}}{Q_{\mathrm{e}}} \tag{1}$$

where $\overline{T}_{\mathrm{cp}} = 0.5\left(T_{\mathrm{out}} + T_{\mathrm{in}}\right)$ is the average cold plate temperature, and T_{in} and T_{out} are the temperature at the inlet and outlet of the cold plate, respectively. Q_{e} is the heat load on the evaporator.

Fig. 10 indicates an obvious difference in the operating temperature and thermal resistance for the cases of various heat loads and configurations. In Fig. 10 (a), the operating temperature after removing the periodic acceleration under configuration B could be higher or lower than that before applying the periodic acceleration although the operating conditions were the same. Apparently, the same operating temperature could also occur. It should be random that there was a stable operating temperature difference. Possible reasons could be attributed to that the history of the periodic acceleration force acting could change the vapor-liquid distribution and the heat leak from the evaporator to the CCs. Furthermore, the stable operating temperature increased under the most working cases, especially at 250 W and 300 W after removing the acceleration patterns. It should be noted that the operating temperature at 150 W under configuration A exceeded the allowable value after removing the acceleration patterns. Therefore, the corresponding data did not be displayed in Fig. 10 (a).

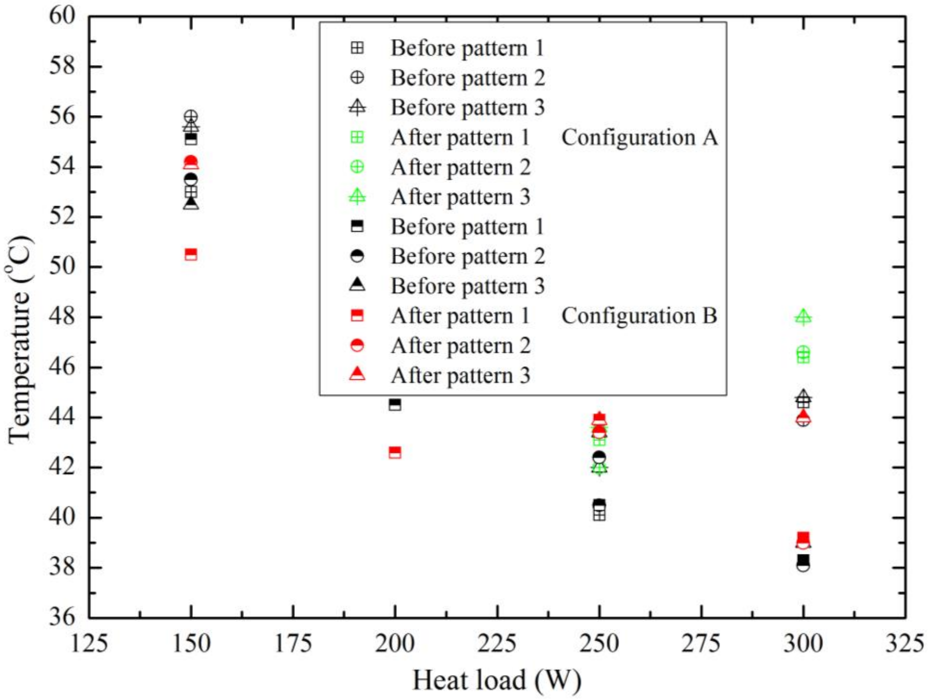

(a) Operating temperature

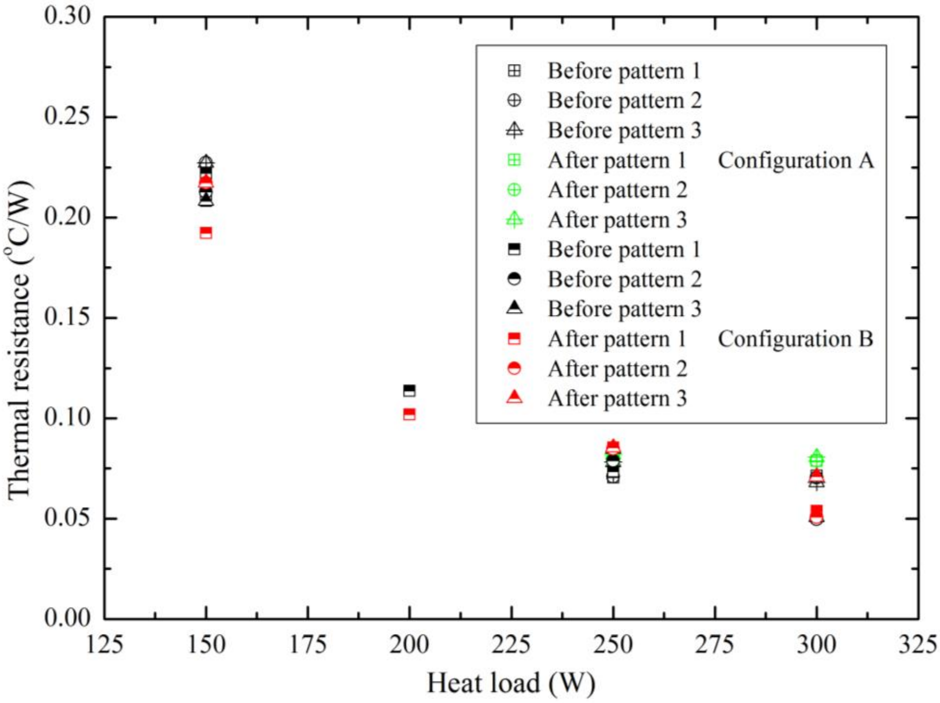

(b) Thermal resistance

Fig. 10 Stable operating temperature and thermal resistance *vs* heat load under all acceleration patterns and configurations at loading mode 1.

As can be seen from Fig. 10 (b), the thermal resistance value decreased with the increase of the heat load for each acceleration pattern and configuration. The maximum value of the thermal resistance was 0.23 ºC/W at 150 W and configuration A before applying periodic acceleration pattern 2. The minimum value was 0.05 ºC/W at 300 W and configuration B before applying periodic acceleration pattern 2. The thermal resistance value after removing the acceleration patterns was higher than that before applying the acceleration patterns for the most working cases.

3.3 Temperature overshooting after unloading

For the cases at loading mode 2 with large heat load, the operating temperature of the DCCLHP could significantly overshoot after the periodic acceleration force was removed. Fig. 11 presents the temperature evolutions at 300 W, periodic acceleration pattern 2 and loading mode 2 under configuration B. The heat load and the acceleration were applied simultaneously at about 278 s. The DCCLHP started up immediately. The acceleration force resulted in the change of the vapor-liquid distribution in the loop. As more liquid entered into the CC1, the heat leak from the evaporator to the CC1 decreased and the RTD1 and RTD2 temperature rose slowly. After the loop started up, the temperature oscillation of the partial loop occurred except for RTD1 and RTD2 points. The evaporator temperature amplitude was the smallest while the amplitude of the liquid line was the largest during the periodic acceleration force acting. The evaporator temperature was approximate 37.3 ºC. Furthermore, the higher the acceleration magnitude, the larger the temperature amplitude of each point.

As the acceleration was removed at 2260 s, there was an obvious peak on the temperature curves of the evaporator, vapor line and CC2, while there was an apparent valley value on the temperature curves of the liquid line and CC1. The peak value of the operating temperature reached 43.7 ℃. After the peak, the temperature of the evaporator, CC2 and vapor line continuously increased. Finally, the loop achieved a steady state. The final operating temperature was about 46.9 ℃. At this time, the vapor-liquid interface in the condenser located somewhere between RTD7 and RTD8.

The similar phenomenon was shown in Fig. 12 for the case of 300 W, periodic acceleration pattern 3 and loading mode 2 under configuration B. The acceleration effect caused the variation of the vapor-liquid distribution at the first 3 g just like that shown in Fig. 11. Temperature oscillations of the evaporator, CC2, vapor line and condenser occurred except for the CC1. The amplitudes of the evaporator and liquid line temperature were still the smallest and largest, respectively. Moreover, the temperature amplitude of both components showed a stepped increase along with the stepped increase of the acceleration magnitude and reached the maximum values at 11 g. Subsequently, the temperature amplitude showed a stepped drop with the stepped decrease of the acceleration magnitude. The operating temperature was about 38 °C under periodic acceleration conditions.

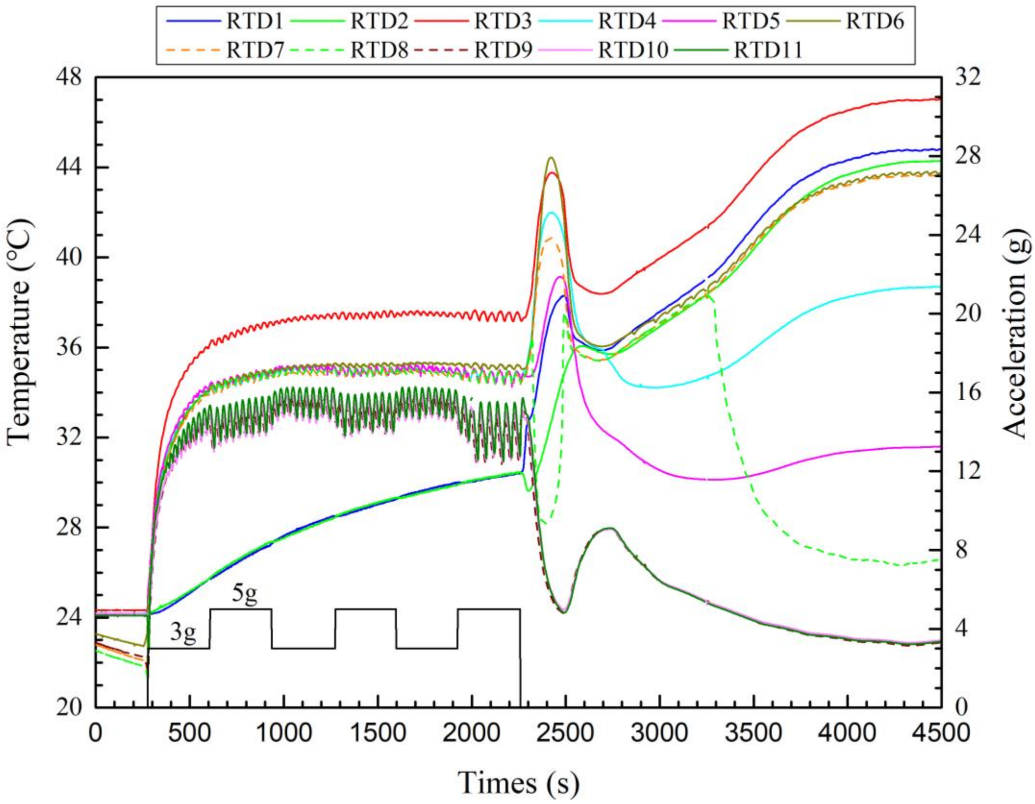

Fig.11 Temperature evolutions at 300 W, acceleration pattern 2 and loading mode 2 under configuration B.

After the periodic acceleration was removed at 3250 s, the evaporator, vapor line and CCs temperature curves presented a formation of an obvious peak. Especially for the vapor line temperature, its instant maximum value got to 50.8 ºC. But the temperature of the liquid line formed a valley. The vapor-liquid interface located somewhere between RTD7 and RTD8 according to their temperatures.

In the current study, it was found that the temperature overshooting also appeared in the periodic acceleration pattern 2 and 3 at 250W with the same loading mode. To be sure, the temperature overshooting under these conditions was negative for the operation of the DCCLHP. The reason for this result could be the variation of the pressure difference in the external loop and the redistribution of the working fluid in the entire loop after unloading acceleration force. As a consequence, the heat leak from the evaporator to CCs and the evaporator temperature increased rapidly.

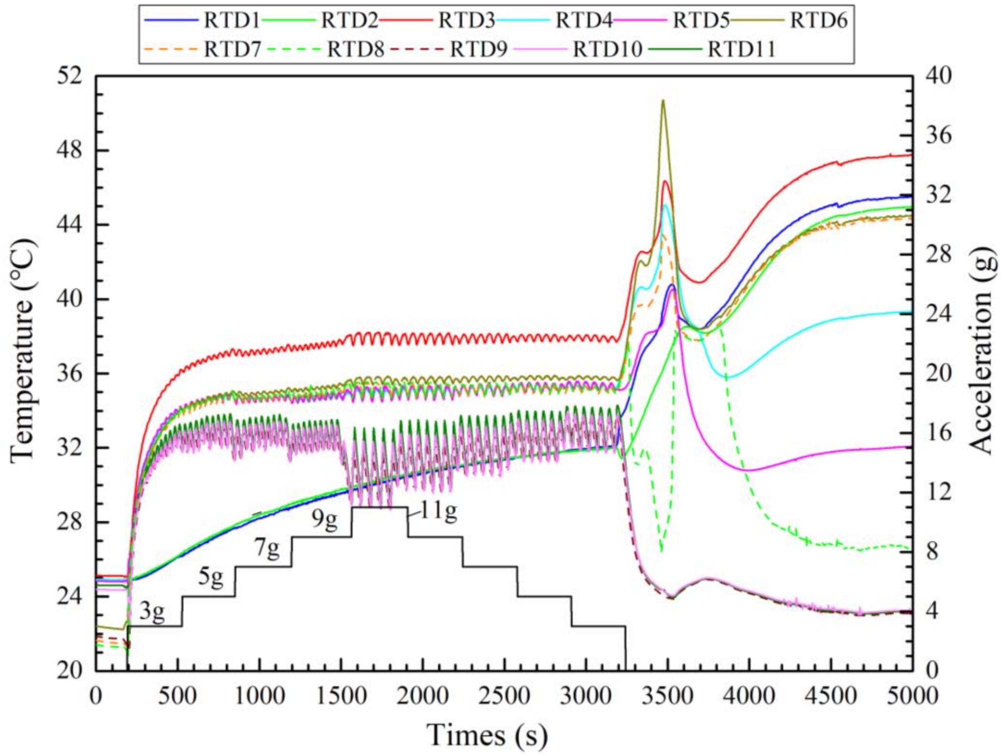

Fig.12 Temperature variations at 300 W, acceleration pattern 3 and loading mode 2 under configuration B.

Fig.13 depicts temperature evolutions at 150 W, acceleration pattern 3 and loading mode 2 under configuration B. The data in Fig. 13 indicates that there was no temperature overshooting after unloading the periodic acceleration. The temperature variation at periodic acceleration pattern 2 was similar to that shown in Fig. 13 under 150 W, loading mode 2 and configuration B. The temperature overshooting might be related to the magnitude of the heat load. The larger the heat load was, more likely the temperature overshooting occurred.

During the periodic acceleration, the temperature of RTD3 to RTD7 showed slightly stepped changes along with stepped increase and decrease of the acceleration force. However, the temperature of the CC1 and liquid line had no stepped changes. The highest temperature of the evaporator reached 37.9 °C when the acceleration was 11 g. The vapor-liquid interface located somewhere between RTD7 and RTD8 point. After the acceleration force was removed at 3058s, the evaporator temperature descended firstly and then rose continuously to approximately 6 ºC. Moreover, the vapor-liquid interface located somewhere between RTD6 and RTD7 point.

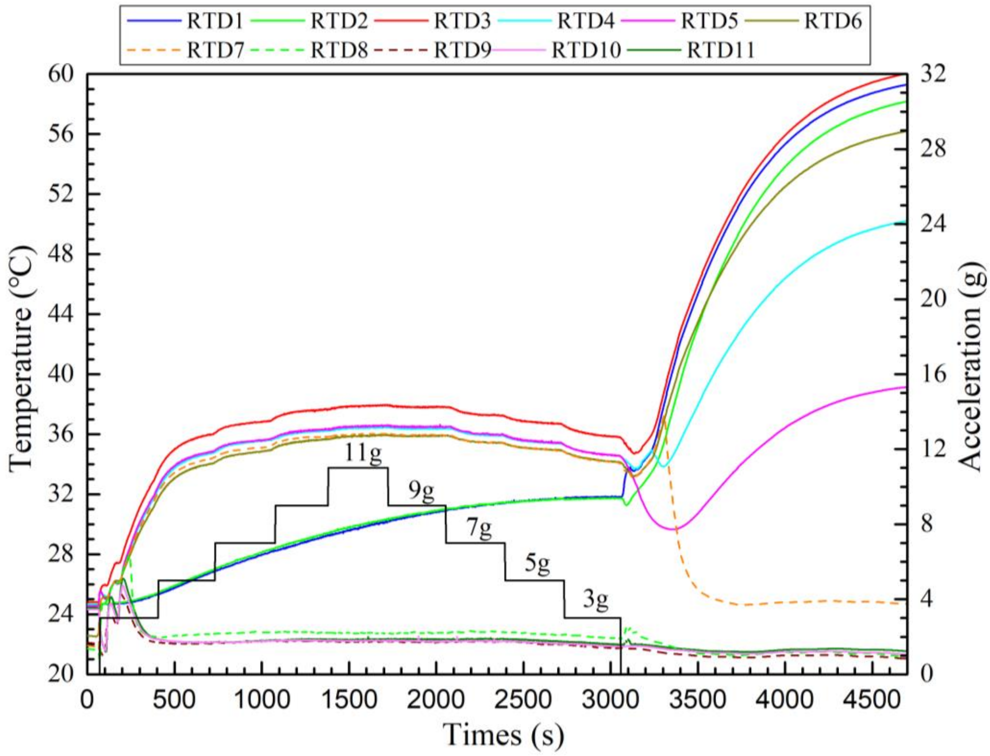

Fig.13 Temperature evolutions at 150 W, acceleration pattern 3 and loading mode 2 under configuration B.

3.4 Temperature oscillation

Besides the periodic change of the loop temperature along with the periodic acceleration force changing, temperature oscillations of the loop during each periodic acceleration were observed in many cases, such as the cases of periodic acceleration pattern 2 or 3 and loading mode 2 at 250 W under configuration A, as well as periodic acceleration pattern 1 or 2 and loading mode 1 at 300 W under configuration B.

Fig. 14 illustrates the loop temperature curves at 300 W, periodic acceleration pattern 1 and loading mode 1 under configuration B. As can be clearly seen from the figure, all the loop temperature except for CC1 temperature showed obvious oscillations during the periodic acceleration force acting. The evaporator temperature at 5 g periodic acceleration was slightly higher than that at 3 g periodic acceleration. The temperature amplitude of the liquid line was greater than that of other loop components. The temperature change of the loop was the largest between both periodic accelerations.

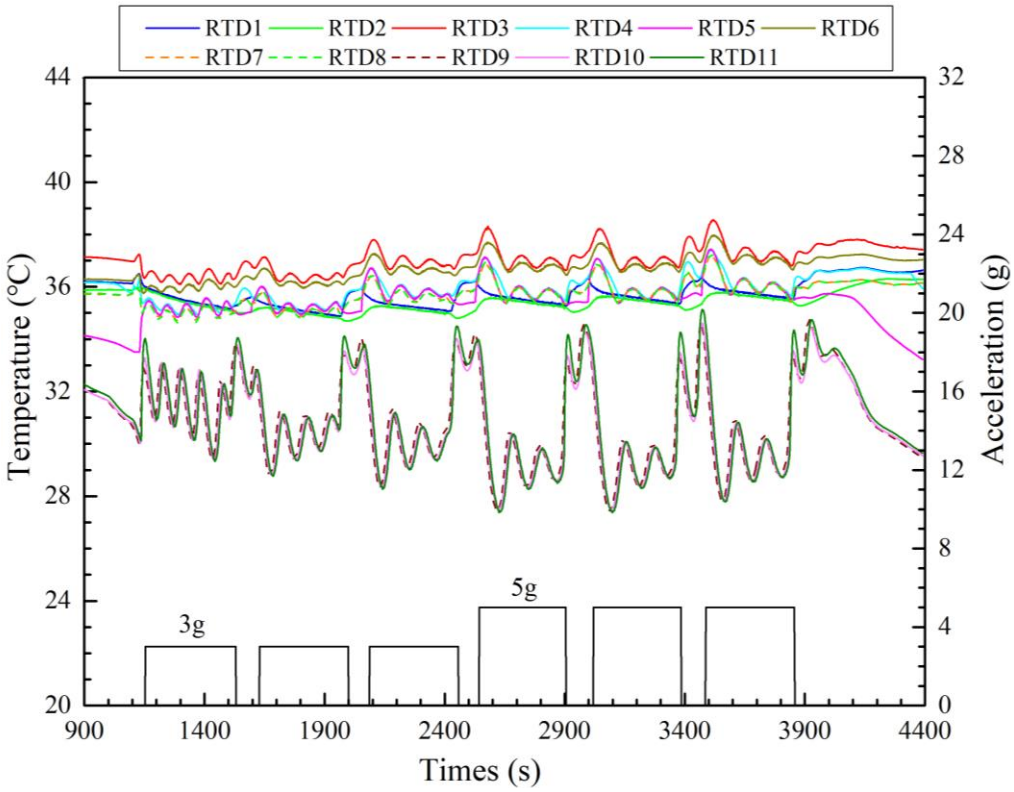

Fig.14 Temperature profiles at 300 W, acceleration pattern 1 and loading mode 1 under configuration B.

It could be confirmed that the effect of the acceleration force led to the temperature oscillation of the loop. The reason could be as follows. The tangential and radial acceleration force changed the vapor-liquid distribution in the loop immediately once it was applied. The heat leak from the evaporator to CC1 reduced but that to CC2 increased a bit. Simultaneously, the pressure head originated from the acceleration force would decrease as the vapor-liquid interface in the condenser moved forward by the increase of the RTD9, RTD10 and RTD11 temperatures. When the RTD9 temperature reached a peak value at about 1138 s, the acceleration pressure head might arrive the smallest value. The capillary pressure difference decreased to the smallest value to balance the loop pressure, which required the RTD4 temperature to drop to a valley value. Simultaneously, the evaporator temperature also decreased and reached a valley value. When the subcooling of the returning liquid could not balance the heat leak, the CC2 temperature stopped to drop and started to rise.

During the following fluctuation period, the vapor-liquid interface started to move backward in the condenser. Therefore, the additional liquid in the CCs took over the space left by the vapor recession through the bayonet. As the interface moved backward in the condenser, the acceleration pressure head increased gradually. Correspondingly, the capillary pressure difference increased to balance the loop pressure. The RTD4 temperature rose. In this process, there was a phase difference between RTD4 and RTD9 temperature. Subsequently, the RTD4 temperature rose to a peak value and then dropped back to a valley value. On the contrary, the RTD9 temperature decreased to a valley value and then increased to a peak value. At this time, the phase difference of the RTD4 and RTD9 temperature disappeared. Then the next cycle of the loop started. As a result, the sustained variation of the external loop pressure and the capillary pressure self-regulation were the essential cause for the temperature oscillation.

In addition, the similar temperature oscillations during each acceleration force acting had been presented in Fig. 11 and Fig. 12. There were significant distinctions in frequency and amplitude between Fig. 11 and Fig. 12 and Fig. 14. It could be caused by the different loading modes and periodic acceleration patterns.

3.5 Excessive operating temperature

In some cases, the operating temperature of the DCCLHP continued to increase and finally exceeded the maximum allowable temperature since the periodic acceleration was applied. Moreover, the excessive operating temperature occurred only at the heat load of 150 W under configuration A.

Fig.15 depicts the temperature curves at 150 W, periodic acceleration pattern 1 and loading mode 1 under configuration A. It could be clearly seen from Fig. 15 that the loop temperature showed a periodic fluctuation during the periodic acceleration. The CC2 temperature presented more significant fluctuation than other components' temperature. The temperature of the CC1, evaporator and vapor line increased gradually during the periodic acceleration acting.

The stable operating temperature was 53 °C in terrestrial gravity and the vapor-liquid interface in the condenser located somewhere between RTD6 and RTD7. When the first 3 g was applied, the liquid with lower temperature filled into the CC2 while the vapor entered into the CC1. The vapor-liquid distribution in the CCs led to an increase of the heat leak from the evaporator to CC1 but a decrease to CC2. However, the subcooling of the returning liquid barely changed. Thus, the CC2 temperature dropped and the CC1 temperature rose in general.

In addition, the acceleration pressure head resulted in the decrease of the external pressure drop. Therefore, the capillary pressure difference reduced. The role of both effects determined the temperature of the evaporator and CC1 descending slightly. After unloading the first 3 g, the RTD4 temperature rose sharply. The RTD5 temperature decreased first and followed by a rapid increase. The temperature change was caused by the vapor-liquid redistribution in the CCs. Additionally, the external loop pressure drop increased which consequently led to a temperature increase of the evaporator and CC1. When the acceleration increased to 5 g, the amplitude of the CC2 temperature became much larger than that at 3 g. Furthermore, the RTD7 temperature increased at 5 g. It indicates that the vapor-liquid interface moved forward in the condenser. Finally, the operating temperature exceeded the safety temperature limit.

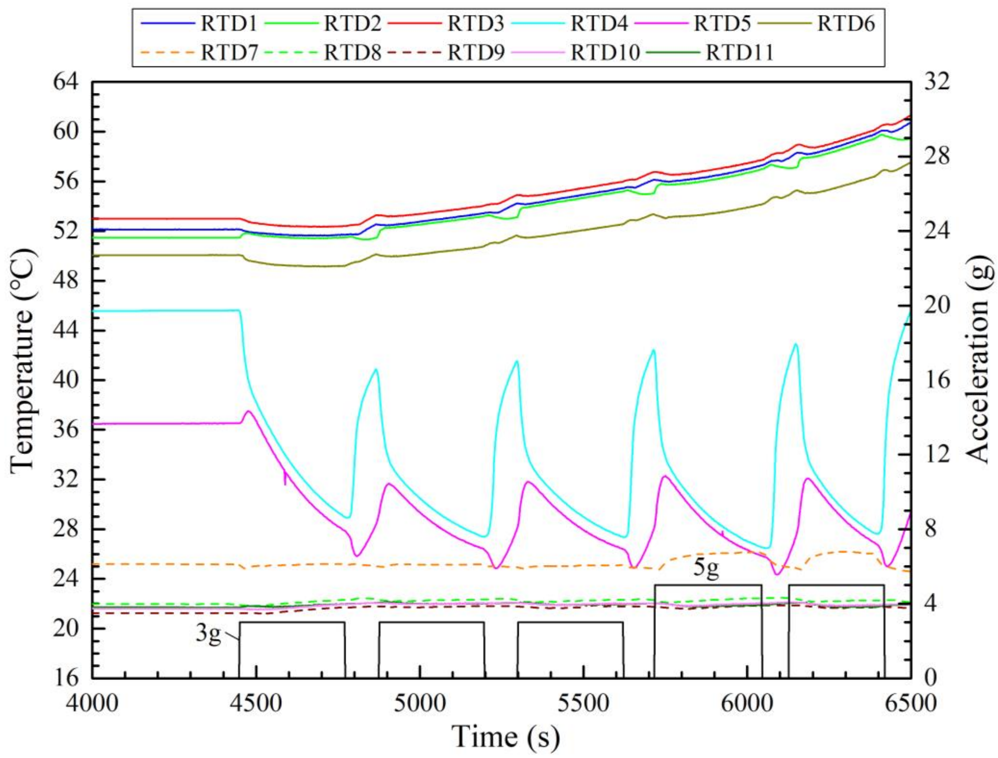

Fig.15 Temperature profiles at 150 W, acceleration pattern 1 and loading mode 1 under configuration A.

Fig.16 displays the temperature curves at 150 W, periodic acceleration pattern 3 and loading mode 2 under configuration A. It demonstrates that the evaporator temperature continuously increased to 62.9 °C. At loading mode 2, the effect of the acceleration force made the CC2 be filled by liquid but the CC1 be filled by vapor. Thereby the heat leak from the evaporator to CC2 decreased but that to CC1 increased. The subcooling of the returning liquid remained constant because the RTD9 temperature was constant. As a consequence, the temperature of the evaporator and CC1 would rise. Moreover, the acceleration pressure head changed along with the vapor-liquid interface moving backward. The evaporator and CC1 temperature continuously increased to regulate the capillary pressure force and further to balance the external loop pressure drop. Meanwhile, the heat leak needed to be balanced by the subcooling of the returning liquid. Finally, the loop failed to reach a steady state.

In the current work, excessive operating temperature was observed only at 150 W under configuration A. It indicated that the phenomenon would be related to the magnitude of the heat load and acceleration direction.

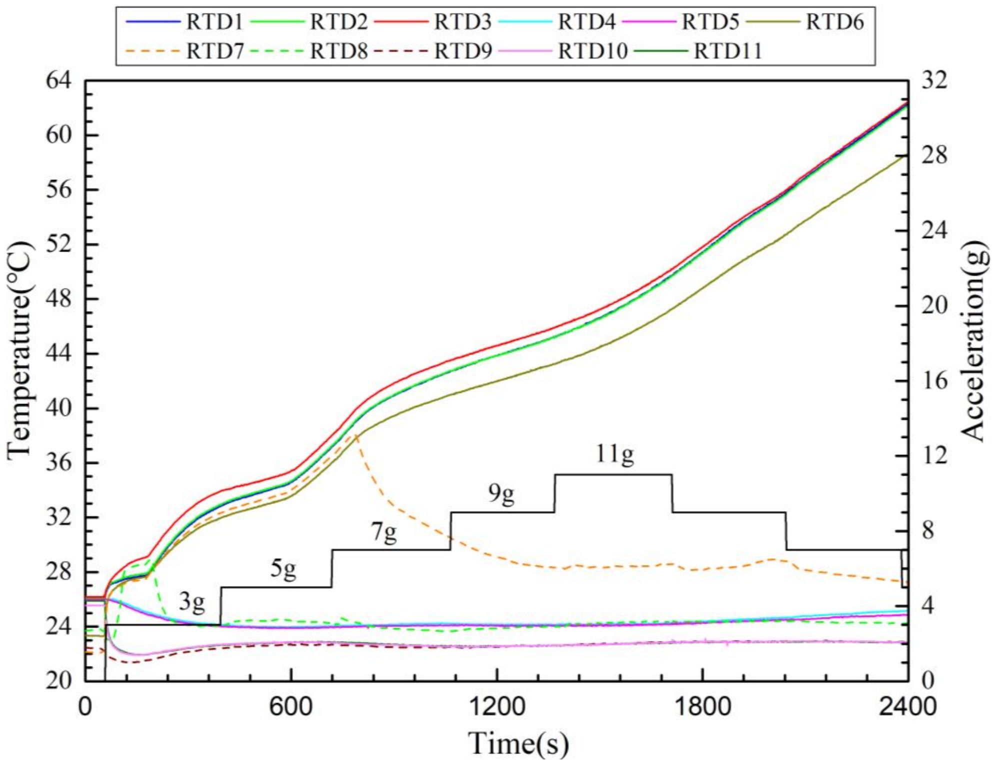

Fig.16 Temperature profiles at 150 W, acceleration pattern 3 and loading mode 2 under configuration A.

4. Conclusions

The operating characteristics of the DCCLHP under periodic acceleration conditions were investigated experimentally in detail. Different heat loads, periodic acceleration patterns, loading modes and acceleration directions were systematically analyzed. The main conclusions are summarized as follows:

(1) During the period of periodic acceleration, the loop temperature periodically oscillated

with the acceleration periodic change. The temperature oscillation at the acceleration pattern 1 was more obvious than that at the acceleration pattern 2 and 3. The higher the acceleration magnitude, the higher the operating temperature. For a given loading mode, heat load and acceleration pattern, the maximum operating temperature under configuration A was greater than that below 40 $^{\circ}$C under configuration B. The maximum operating temperature dropped with the heat load increasing under configuration A. But it dropped firstly and then rose under configuration B. The maximum operating temperature at the acceleration pattern 3 was the greatest among the three studied patterns.

(2) For the loading mode 1, the stable operating temperature difference and thermal resistance under configuration B occurred randomly between before and after the periodic acceleration force acting. Moreover, the stable operating temperature increased under the most working cases, especially at 250 W and 300 W after removing the acceleration. For the loading mode 2, there was a temperature overshooting after unloading, which could cause the operating temperature exceeding 60 $^{\circ}$C. The larger the heat load was, more likely the temperature overshooting occurred. Both observed phenomena could be explained by the change of the loop vapor-liquid distribution and the heat leak from the evaporator to the CCs.

(3) The loop temperature during each periodic acceleration showed obvious oscillation along with varying the frequency and amplitude in some cases of 250 W and 300 W. The sustained variation of the external loop pressure and the capillary pressure self-regulation were the essential cause for the temperature oscillations. For several cases of 150 W under configuration A, the excessive operating temperature could appear and even more than 60 $^{\circ}$C, which would be related to the heat load and the acceleration direction.

In this study, we demonstrated the operating performance including the above discussed four kinds of particular phenomena, which are the essential factors that must be considered for the DCCLHP system in practical applications. The corresponding analysis and possible mechanism explanation are proposed for the first time, with potential significance of paving a foundation to solve the critical problems of the DCCLHP. Investigating feasible strategies to address such problems is the focus of our further research.

Acknowledgement

The authors acknowledge the financial supports from the Fundamental Research Funds for the Central Universities of China (YWF-14-HKXY-019) and the National Natural Science Foundation of China (No. 11772038).

References

[1] R. Wu, Y. Fan, T. Hong, H. Zou, R. Hu, X. Luo. An immersed jet array impingement cooling device with distributed returns for direct body liquid cooling of high power electronics. Applied Thermal Engineering, 162(2019) 114259.

[2] N. S. Ramasamy, P. Kumar, B. Wangaskar, S. Khandekar, Y. F. Maydanik. Miniature ammonia loop heat pipe for terrestrial applications: Experiments and modeling. International Journal of Thermal Sciences, 124(2018) 263-278.

[3] Q. Su, S. Chang, Y. Y. Zhao, H. Zheng, C. Dang. A review of loop heat pipes for aircraft anti-icing applications. Applied Thermal Engineering, 130(2018) 528-540.

[4] Y. F. Maydanik. Loop heat pipes. Applied thermal engineering, 25(5-6) (2005) 635-657.

[5] Z. Xue, M. Xie, J Duan, W. Qu. Experimental Study of High-Efficiency Loop Heat Pipe for High Power Avionics Cooling. Asia-Pacific International Symposium on Aerospace Technology. Springer, Singapore, (2018) 1865-1871.

[6] S. He, J. Zhao, Z. C. Liu, W. Tian, J. G. Yang, W. Liu. Experimental investigation of loop heat pipe with a large squared evaporator for cooling electronics. Applied Thermal Engineering, 144(2018) 383-391.

[7] M. Nishikawara, K. Otani, Y. Ueda, H. Yanada. Liquid–vapor phase behavior and operating characteristics of the capillary evaporator of a loop heat pipe at start-up. International Journal of Thermal Sciences, 129(2018) 426-433.

[8] Y. H. Yau, M. Ahmadzadehtalatapeh. A review on the application of horizontal heat pipe heat exchangers in air conditioning systems in the tropics. Applied Thermal Engineering, 30(2-3) (2010) 77-84.

[9] G. Zhou, J. Li. Two-phase flow characteristics of a high performance loop heat pipe with flat evaporator under gravity. International Journal of Heat and Mass Transfer, 117(2018) 1063-1074.

[10] A. Ambirajan, A. A. Adoni, J. S. Vaidya, A. A Rajendran, D. Kumar, P. Dutta. Loop heat pipes: a review of fundamentals, operation, and design. Heat Transfer Engineering, 33(4-5)

(2012) 387-405.
[11] X. Li, K. Zhu, H. Li, X. Chen, Y. Wang. Performance comparison regarding loop heat pipes with different evaporator structures. International Journal of Thermal Sciences, 136(2019) 86-95.
[12] X. Chang, N. Watanabe, H. Nagano. Operating Visualization study of a loop heat pipe with two evaporators and one condenser under gravity-assisted condition. International Journal of Heat and Mass Transfer, 135(2019) 378-391.
[13] K. Ishii, K. Fumoto. Temperature visualization and investigation inside evaporator of pulsating heat pipe using temperature-sensitive paint. Applied Thermal Engineering, 155(2019) 575-583.
[14] D. Gluck, C. Gerhart, Stanley S. Characterization of a high capacity, dual compensation chamber loop heat pipe, AIP Conference Proceedings, 458(1) (1999) 943-948.
[15] C. Gerhart, D. Gluck. Summary of operating characteristics of a dual compensation chamber loop heat pipe in gravity, The 11th International Heat Pipe Conference, Tokyo, Japan, (1999) 67-68.
[16] J. B. Long, J. M. Ochterbeck. Transient/cyclic heat loads for dual compensation chamber loop heat pipes, Proceedings of XIIHPC, Japan Association for Heat Pipes, (1999) 305-310.
[17] G. Lin, H. Zhang, X. Shao, J. Cao, T. Ding, J. Miao. Development and test results of a dual compensation chamber loop heat pipe. Journal of thermophysics and heat transfer, 20(4) (2006) 825-834.
[18] L. Bai, G. Lin, D. Wen, J. Feng, Experimental investigation of startup behaviors of a dual compensation chamber loop heat pipe with insufficient fluid inventory. Applied Thermal Engineering, 29(8-9) (2009) 1447-1456.
[19] J. Feng, G. Lin, L. Bai. Experimental investigation on operating instability of a dual compensation chamber loop heat pipe. Science in China Series E: Technological Sciences, 52(8) (2009) 2316-2322.
[20] G. Lin, N. Li, L. Bai, D. Wen. Experimental investigation of a dual compensation chamber loop heat pipe. International Journal of Heat and Mass Transfer, 53(15-16) (2010) 3231-3240.

[21] Y. Zhao, S. Chang, B. Yang, W. Zhang, M. Leng. Experimental study on the thermal performance of loop heat pipe for the aircraft anti-icing system. International Journal of Heat and Mass Transfer, 111(2017) 795-803.

[22] Q. Su, S. Chang, M. Song, Y. Zhao, C. Dang. An experimental study on the heat transfer performance of a loop heat pipe system with ethanol-water mixture as working fluid for aircraft anti-icing. International Journal of Heat and Mass Transfer, 139(2019) 280-292.

[23] J. Ku, L. Ottenstein, T. Kaya, P. Rogers, C. Hoff. Testing of a loop heat pipe subjected to variable accelerating forces, part 1: start-up, SAE Technical Paper, 2000.

[24] J. Ku, L. Ottenstein, T. Kaya, P. Rogers, C. Hoff. Testing of a loop heat pipe subjected to variable accelerating forces, Part 2: Temperature stability. SAE Technical Paper, 2000.

[25] A. J. Fleming, S. K. Thomas, K. L. Yerkes. Titanium-water loop heat pipe operating characteristics under standard and elevated acceleration fields. Journal of Thermophysics and Heat Transfer, 24(1) (2010) 184-198.

[26] K. L. Yerkes, J. D. Scofield, D. L. Courson, H. Jiang. An experimental investigation into the transient performance of a titanium-water loop heat pipe subjected to a steady-periodic acceleration field.50th AIAA Aerospace Sciences Meeting including the New Horizons Forum and Aerospace Exposition. (2012) 1009.

[27] K. L. Yerkes, J. D. Scofield, D. L. Courson, H. Jiang. Steady-periodic acceleration effects on the performance of a loop heat pipe. Journal of Thermophysics and Heat Transfer, 28(3) (2014) 440-454.

[28] K. L. Yerkes, J. D. Scofield, D. L. Courson. Performance of a loop heat pipe subjected to a phase-coupled heat input to an acceleration field. 46th AIAA Thermophysics Conference, (2016) 4145.

[29] Y. Xie, J. Zhang, L. Xie, Y. Yu, H. Wu, H. Zhang, H. Gao. Experimental investigation on the operating characteristics of a dual compensation chamber loop heat pipe subjected to acceleration field. Applied Thermal Engineering, 81(2015) 297-312.

[30] Y. Xie, Y. Zhou, D. Wen, H. Wu, G. Haritos, H. Zhang. Experimental investigation on transient characteristics of a dual compensation chamber loop heat pipe subjected to acceleration forces. Applied Thermal Engineering, 130(2018) 169-184.